Computer Modeling in Engineering & Sciences
DOI:10.32604/cmes.2020.010796
Article

Exploring the Abnormal Brain Regions and Abnormal Functional Connections in SZ by Multiple Hypothesis Testing Techniques

Lan Yang[1], Shun Qi[2,3,#], Chen Qiao[1,*] and Yanmei Kang[1]

[1]School of Mathematics and Statistics, Xi'an Jiaotong University, Xi'an, 710049, China
[2]Department of Radiology, The First Affiliated Hospital of Medical College, Xi'an Jiaotong University, Xi'an, 710061, China
[3]Department of Radiology, Xijing Hospital, Fourth Military Medical University, Xi'an, 710032, China
[*]Corresponding Author: Chen Qiao. Email: qiaochen@xjtu.edu.cn
[#]The co-first author
Received: 30 March 2020; Accepted: 29 June 2020

Abstract: Schizophrenia (SZ) is one of the most common mental diseases. Its main characteristics are abnormal social behavior and inability to correctly understand real things. In recent years, the magnetic resonance imaging (MRI) technique has been popularly utilized to study SZ. However, it is still a great challenge to reveal the essential information contained in the MRI data. In this paper, we proposed a biomarker selection approach based on the multiple hypothesis testing techniques to explore the difference between SZ and healthy controls by using both functional and structural MRI data, in which biomarkers represent both abnormal brain functional connectivity and abnormal brain regions. By implementing the biomarker selection approach, six abnormal brain regions and twenty-three abnormal functional connectivity in the brains of SZ are explored. It is discovered that compared with healthy controls, the significantly reduced gray matter volumes are mainly distributed in the limbic lobe and the basal ganglia, and the significantly increased gray matter volumes are distributed in the frontal gyrus. Meanwhile, it is revealed that the significantly strengthened connections are those between the middle frontal gyrus and the superior occipital gyrus, the superior occipital gyrus and the middle occipital gyrus as well as the middle occipital gyrus and the fusiform gyrus, and the rest connections are significantly weakened.

Keywords: Multiple hypothesis testing; schizophrenia; magnetic resonance imaging; abnormal brain regions; abnormal functional connectivity

1 Introduction

Schizophrenia (SZ) is one of the most complex mental diseases, which may lead to disturbance of emotion, delusion of persecution, disorder of consciousness, abnormal behavior and deficits in cognitive functions [1]. Recently, magnetic resonance imaging (MRI) techniques which include functional MRI and structural MRI has been widely used in studying SZ. The functional MRI which measures spontaneous low-frequency fluctuations in blood oxygen level-dependent signal in subjects can study the functional activities of different brain regions, especially the correlation of functional activities with time. The

structural MRI scans the gray matter, white matter and cerebrospinal fluid based on the anatomical structure of human brains to check if the brain tissue is damaged, and it provides an anatomical basis for the study of functional connectivity. With the extensive use of MRI techniques, many researches have provided us with some understanding of the neurobiological mechanisms underlying its symptoms of schizophrenia [2,3]. For example, Zalesky et al. [4] found evidence of disconnection in white-matter connectional architecture in SZ, and which suggests that functional disconnections in SZ might be the result of multifaceted pathophysiology involving both axonal in addition to putative synaptic mechanisms. Chang et al. [5] found that schizophrenia, bipolar disorder, major depressive disorder and healthy controls had significant differences in gray matter volumes in the paralimbic and heteromodal cortices. Sui et al. [2] demonstrated that the salience network, *corpus* callosum, central executive and default-mode networks can be considered as modality-specific biomarkers of generalized cognition. Du et al. [6] suggested that early illness SZ patients showed both increasing and decreasing connectivity, mainly hypo-connectivity involving 15% of the altered voxels from four intrinsic functional networks. Crimi et al. [7] found widespread connectivity cortical and sub-cortical differences in patients with schizophrenia compared to controls by using the multi-link analysis. These studies on developing biomarkers allow the field of imaging analysis and psychiatry to move forward.

Because SZ is often accompanied by cognitive decline, it seems necessary to understand the underlying neural mechanism of SZ by analyzing the functional and structural MRI data. However, for the MRI data, the sample size is usually smaller than the feature numbers, in which redundant and irrelevant features and noises are intensive, thus this property makes it difficult to find the potential information contained in the data from a limited number of observations that form a cognitive concept of the data or complete identification task [8]. To discover the potential information from the data which has a smaller sample size than feature numbers, the commonly used approach is dimension reduction which includes feature selection and feature extraction. As the two most commonly used dimension reduction methods for high-dimensional data, feature selection and feature extraction are quite different. Feature extraction is to transform the original space into a new space with different bases. The common methods of feature extraction include deep learning, principal component analysis, factor analysis, linear discriminant analysis and singular value decomposition. Since the original data can no longer be interpreted and read directly after being transformed into a new space, feature extraction is usually only used in classification analysis. The feature selection is based on certain rules, such as the evaluation index of the classifier, the dimension of the selected feature subset, the conditional probability distribution function of the data, the selected feature subset remain unchanged and etc, and then directly select a subspace from the original space. In the process of feature selection, those redundant and invalid features will be removed as much as possible, and the features corresponding to the key information of the original data set will be retained at the same time, and the retaining feature set is composed of the key original features that can distinguish different categories. Since the data can be direct interpretability in the original space after feature selection, feature selection is widely used in many fields such as time series prediction, medical image analysis, speech recognition, computer vision, information retrieval [9–12].

Statistical indicators such as correlation coefficient, hypothesis testing and mutual information are often used in the feature selection process [13]. The correlation coefficient selects features by calculating the correlation coefficients between each feature and output in all training sets and setting a threshold to filter the features with a lower correlation than the threshold. Hypothesis testing such as the χ^2-test, the F-test and the t-test can test the correlations between each feature and output and get the p-values, and then set a threshold to filter the features with greater p-values than the threshold. Furthermore, hypothesis testing can be divided into two categories, i.e., single hypothesis testing and multiple hypothesis testing. The multiple hypothesis testing is often used to test more than one hypothesis within a single analysis and it can inflate the type 1 error rate (i.e., the probability of erroneously rejecting true null hypotheses) within a study [14]. Compared with multiple hypothesis testing, single hypothesis testing fails to test a large

number of hypotheses simultaneously due to the type 1 error will increase rapidly as the number of tests raises, especially in high dimensional situations.

In the procedure of the multiple hypothesis testing, there are two main types called frequentist approaches and empirical Bayes approaches [15]. The frequentist approaches treat the parameter to be inferred as a fixed and unknown constant and estimate the number of the true null hypothesis m_0 from the data directly. Among the frequentist approaches, Hochberg et al. [16] proposed the method which concretized and implemented the graphical method proposed by Schweder et al. [17]. Then motivated by the previous work [16–18], Benjamini et al. [19] proposed the adaptive procedure which is more powerful in controlling the expected ratio of the number of erroneous rejections to the number of rejections (i.e., false discovery rate, FDR) and is beneficial for the dependent case and has the property of unbiasedness due to the m_0 estimated by the unbiased maximum likelihood estimator. Besides, to further improve the power in the procedure of controlling the FDR, Storey proposed the method based on the bootstrap approach [20] which aimed at fixing the rejection region and then estimated the corresponding error rate. Because the method based on the bootstrap approach [20] has higher computational complexity as the number of hypotheses increases, Storey et al. [21] proposed the method which replace the bootstrap approach with the natural cubic spline approach. The empirical Bayes approaches assume that the test statistic t has a mixture density $f(t) = \pi_0 f_0(t) + (1 - \pi_0) f_1(t)$ where π_0 is the true null hypotheses m_0 to all null hypotheses m ratio (i.e., $\pi_0 = \frac{m_0}{m}$) and then use an empirical null distribution to estimate m_0 from the data. Among the empirical Bayes approaches, Strimmer [22] proposed a unified method based on a modified Grenander density estimator, and this method was semiparametric. Moreover, Liang and Zhang proposed the method which used a mixture of exponential power distribution to model $f(t)$ and then estimated π_0 using the stochastic approximation algorithm.

Motivated by identifying the biomarkers of SZ that are associated with the cognitive composite ability and the specific cognitive domains such as attention, working memory, and verbal learning, in this paper, we explore the brain abnormalities of SZ by proposing the biomarker selection approach based on the multiple hypothesis testing techniques which combine both frequentist approaches and empirical Bayes approaches. The data with 410 features has 40 patients with SZ and 46 healthy controls (HCs), and there are 32 features from the structural MRI (i.e., source-based morphometric, SBM) and the rest features from the functional MRI (i.e., functional network connectivity, FNC). By applying our approach to the data set, the results show that there exist six aberrant brain regions and 23 abnormal connectivity between the SZ group and HCs group. These abnormal brain regions are located in the cingulate gyrus, middle frontal gyrus, parahippocampal gyrus, precuneus, superior frontal gyrus and caudate, where the gray matter volumes of the cingulate gyrus, parahippocampal gyrus, precuneus and caudate significantly reduced and the gray matter volumes of the frontal gyrus significantly increased. Among the 23 abnormal connectivity, the five regions with the most connections are rolandic operculum, middle frontal gyrus, insula, lingual gyrus and caudate, and most of the abnormal connections in SZ group significantly reduced compared with HCs group. Furthermore, we compare our approach with the other two methods and use the network analysis based on graph theory to show the validity of our approach and confirm the significance of the selected biomarkers. The results indicate that the selected biomarkers are basically consistent with the previous literature [23–25] and confirm that the selected biomarkers are significant. Because the volumes of the gray matter can reflect whether the brain tissue is damaged and the ability of the functional connectivity between different brain regions can reflect the degree of brain disorders, the selected biomarkers can reveal the abnormal neural mechanism of the brain disease, serve for the accurate medical treatment of the disease, improve the accurate diagnosis ability of the brain disease and guide the clinical intervention and treatment such as transcranial magnetic stimulation.

2 Methodology

In this section, we will introduce the multiple hypothesis testing techniques, and six methods based on the multiple hypothesis testing techniques will be introduced which can control the FDR at a level α. Then we will propose a biomarker selection approach to find the significant difference between SZ group and healthy controls which combine these six methods. Moreover, the network analysis based on graph theory will be presented to show the validity of the approach proposed here.

2.1 Background of the Multiple Hypothesis Testing Techniques

Hypothesis testing techniques play an important role in the statistical inference, and it can be divided into two types, i.e., single hypothesis testing and multiple hypothesis testing, where the multiple hypothesis testing tests several hypotheses simultaneously and the single hypothesis testing only tests one hypothesis. There are two hypotheses called the null hypothesis and the alternative hypothesis involving in the hypothesis testing, and the type 1 error is that the null hypothesis is true but we reject it, and the type 2 error is that the null hypothesis is not true but we do not reject it. In the single hypothesis testing, Neyman et al. [26] proposed that we should seek a test to make the probability of occurring the type 1 error within a certain range, while the probability of occurring the type 2 error is as small as possible. However, the type 1 error will increase rapidly as the number of tests raises, therefore, it is invalid to use the principle proposed by Neyman and Pearson in the multiple hypothesis testing. In order to solve this problem, many principles have been proposed, such as the family-wise error rate (FWER), false discovery rate (FDR), positive false discovery rate (pFDR) and marginal false discovery rate (mFDR) [27].

Assuming that there are m null hypotheses $H_1, H_2,\ldots, H_m$ with corresponding m p-values $p_1, p_2,\ldots, p_m$, and in the process of significant testing, the null hypotheses are considered to be statistically significant when their corresponding p-values are less than or equal to the threshold $\alpha \in (0,1]$. Usually, the threshold is 0.05 or 0.01, but it can be fixed by requirements for the accuracy of the test. And the outcomes are shown in the Tab. 1 when the procedure is conducted to obtain which of the m hypotheses are statistically significant. More precisely, Tab. 1 describes the possible results in different situations, where V represents the number of tests that the type 1 error happens, T represents the number of tests that the type 2 error happens and R represents the number of significant null hypotheses. According to the Tab. 1, FWER, FDR, pFDR and mFDR are defined as Eqs. (1)–(4).

$$FWER = Pr(V \geq 1), \tag{1}$$

$$FDR = E\left[\frac{V}{R \vee 1}\right] = E\left[\frac{V}{R}|R > 0\right]Pr(R > 0), \tag{2}$$

$$pFDR = E\left[\frac{V}{R}|R > 0\right], \tag{3}$$

$$mFDR = \frac{E[V]}{E[R]}. \tag{4}$$

Remarkably, under the condition that all null hypotheses are true, $pFDR = mFDR = 1$ holds, whereas FDR can be any value in the closed interval [0,1] due to the item $Pr(R > 0)$. Compared with the FWER, the testing criterion of the FDR is more relaxed, and FDR can be used as an evaluation index for selecting the significant variables, while FWER is mainly used to control the type 1 error, therefore, FDR is more commonly used in practice. In the process of the multiple hypothesis testing, FDR control which is to select a data-dependent rule to make the expected FDR less than or equal to the pre-chosen threshold is important for the validity of the test outcome and the approach proposed by Benjamini et al.

Table 1: The various results from the m hypotheses testing obtained by the significant test procedure with the threshold $\alpha \in (0,1]$

	Significant ($p \le \alpha$)	Not significant ($p > \alpha$)	Total
Null True	V	U	m_0
Alternative True	S	T	m_1
Total	R	W	m

p denotes the p-value, V represents the number of tests that the type 1 error happens, U represents the number of tests that the null hypothesis is true and we do not reject it, S represents the number of tests that the null hypothesis is not true and we reject it, T represents the number of tests that the type 2 error happens, R represents the number of the significant null hypotheses, W represents the number of the nonsignificant null hypotheses, m_0 is the number of the true null hypotheses and m_1 is the number of the true alternative hypotheses.

[19] which we called the two-stage BH control is often used owing to the high power. The two-stage BH control approach is that we estimate the number of the true null hypotheses firstly cause that the quality of the estimator of the number of the true null hypotheses has an impact on the power of the significance testing and then we implement the BH control approach [18], and the detail of it is shown in Algorithm 2.1.

Algorithm 2.1 Two-stage BH control algorithm

Input: The observed p-values $p_1, p_2, \ldots, p_m$ related to the hypotheses $H_1, H_2, \ldots, H_{\mathrm{m}}$, the threshold $\alpha \in (0,1]$, the estimator of the number of true null hypotheses $\hat{m}_0$ and the number of hypotheses m.

Output: The corresponding index of $H_{(1)}, H_{(2)}, \ldots, H_{(\hat{k})}$.

1. Calculate α^* by this formula $\alpha^* = \dfrac{\alpha m}{\hat{m}_0}$;
2. Sort the observed p-values as $p_{(1)} \le p_{(2)} \le \cdots \le p_{(m)}$;
3. Calculate $\hat{k}$ by this formula $\hat{k} = max\{1 \le k \le m : p_{(k)} \le \dfrac{k\alpha^*}{m}\}$;
4. If $\hat{k}$ exists, then reject null hypotheses $H_{(1)}, H_{(2)}, \ldots, H_{(\hat{k})}$ relevant to $p_{(1)}, p_{(2)}, \ldots, p_{(\hat{k})}$. Otherwise, reject nothing.

2.2 Multiple Hypothesis Testing Techniques Based on the Frequentist Approaches

Assuming that there are m_0 true null hypotheses among m hypotheses with corresponding ordered p-values $p_{(1)} \le p_{(2)} \le \ldots \le p_{(m)}$. Let $q_{(i)} = 1 - p_{(m+1-i)}$ hold for all $i = 1,2,\ldots,m$ and it means $q_{(1)} \le q_{(2)} \le \ldots \le q_{(m)}$. When all null hypotheses are true, $m_0 = m$ and the distribution of $q_{(i)}$ is same as the ith largest sample from a uniform distribution over [0,1]. Therefore, $E(q_{(i)}) \approx \dfrac{i}{m_0 + 1}$ holds for all $i = 1,2, \ldots, m$ and the slope of the straight line fitted by data $\{(i, q_{(i)})\}_{i=1}^{m}$ is $\dfrac{1}{m_0 + 1}$ approximately. To get the estimator of m_0, the simple way is to obtain the estimator slope of line fitted by these points with small value of $q_{(i)}$, and which is the main idea of the graphical method proposed by Schweder et al. [17] and concretized and implemented by Hochberg et al. [16]. The detail of the multiple hypothesis testing based on the idea of the slope estimator (MHT-SE) is described as Algorithm 2.2.

Algorithm 2.2 MHT-SE

Input: The observed p-values $p_1, p_2, \ldots, p_m$ related to the hypotheses $H_1, H_2, \ldots, H_m$, the threshold $\alpha \in (0, 1]$ and the number of hypotheses m.

Output: The corresponding index of $H_{(1)}, H_{(2)}, \ldots, H_{\widehat{(k)}}$.

1. Sort the observed p-values as $p_{(1)} \leq p_{(2)} \leq \cdots \leq p_{(m)}$;
2. Set $q_{(i)} = 1 - p_{(m+1-i)}$ for all $i = 1, 2, \cdots, m$;
3. Use the ordinary least squares method to obtain the slope estimator $\widehat{\beta}$ of the line fitted by the data points $\{(i, q_{(i)})\}_{i=1}^{m}$;
4. Calculate $\widehat{m}_0$ by formula $\widehat{m}_0 = \left[\frac{1}{\widehat{\beta}} - 1\right]$, where $[\cdot]$ means the biggest integer less than or equal to this number;
5. Repeat the procedure of Algorithm 2.1.

To further enhance the power of the multiple hypothesis testing, Hochberg et al. [19] proposed the method based on the lowest slope estimator to estimate m_0. This method is to estimate the slope between $(i, p_{(i)})$ and $(m + 1, 1)$ for all $i = 1,2, \ldots, m$, and then the smallest value among these slopes are chosen to estimate m_0. And the procedure of the multiple hypothesis testing based on the lowest slope estimator (MHT-LSE) is described as Algorithm 2.3.

Algorithm 2.3 MHT-LSE

Input: The observed p-values $p_1, p_2, \cdots, p_m$ related to the hypotheses $H_1, H_2, \cdots, H_m$, the threshold $\alpha \in (0, 1]$ and the number of hypotheses m.

Output: The corresponding index of $H_{(1)}, H_{(2)}, \ldots, H_{\widehat{(k)}}$.

1. Sort the observed p-values as $p_{(1)} \leq p_{(2)} \leq \cdots \leq p_{(m)}$;
2. Set $S_i = \frac{1 - p_{(i)}}{m + 1 - i}$ for all $i = 1, 2, \ldots, m$, and compute $J = \min\{2 \leq j \leq m : S_j < S_{j-1}\}$;
3. Calculate $\widehat{m}_0$ by formula $\widehat{m}_0 = \min\left\{\left[\frac{1}{S_J} + 1\right], m\right\}$, where $[\cdot]$ means the biggest integer less than or equal to this number;
4. Repeat the procedure of Algorithm 2.1.

Suppose that π_0 is the true null hypotheses to all null hypotheses ratio, and then $m_0 = \pi_0 \times m$ holds. Meanwhile, since the null hypotheses with the larger p-values are more likely to not be rejected, naturally, π_0 can be estimated by Eq. (5),

$$\widehat{\pi}_0(\lambda) = \frac{\sum_{i=1}^{m} I_{(p_i > \lambda)}}{(1 - \lambda)m} = \frac{W(\lambda)}{(1 - \lambda)m}, \tag{5}$$

where $\lambda \in [0,1]$ is a given value and $I_{(\cdot)}$ is an indicator function. And $I_{(pi > \lambda)} = 1$ when $p_i > \lambda$ holds, otherwise, it is zero. By the Eq. (5) and the relation between m_0 and π_0, i.e., $m_0 = \pi_0 \times m$, the estimator $\hat{m}_0$ can be computed. However, how to select an appropriate λ to estimate π_0 is a problem, thus, the selection strategy of λ is proposed by Storey [20] which is to minimize the mean squared error of estimation using the bootstrap approach, and then π_0 is estimated with the optimal λ. And the procedure of the multiple hypothesis testing based on the bootstrap approach (MHT-B) is described as Algorithm 2.4.

Algorithm 2.4 MHT-B

Input: The observed p-values $p_1, p_2, \ldots, p_m$ related to the hypotheses $H_1, H_2, \ldots, H_m$, the threshold $\alpha \in (0, 1]$, the number of hypotheses m and a constant B.

Output: The corresponding index of $H_{(1)}, H_{(2)}, \ldots, H_{\widehat{(k)}}$.

1. For each given λ from $\Lambda = \{0, 0.05, \ldots, 0.9, 0.95\}$, calculate the corresponding value of $\widehat{\pi}_0(\lambda)$ by the Eq. (5) and set $\pi_0^{min} = \min_{\lambda \in \Lambda}\{\widehat{\pi}_0(\lambda)\}$;

2. For each $\lambda \in \Lambda$, bootstrap approach is performed B times to get p_{bi}, $b = 1, 2, \ldots, B$; $i = 1, 2, \ldots, m$, and then calculate $\widehat{\pi}_0^b(\lambda) = \dfrac{\sum_{i=1}^{m} I_{(p_{bi} > \lambda)}}{(1-\lambda)m}$ for $b = 1, 2, \ldots, B$;
3. For each $\lambda \in \Lambda$, compute $\widehat{MSE}(\lambda) = \dfrac{1}{B}\sum_{b=1}^{B} (\widehat{\pi}_0^b(\lambda) - \pi_0^{min})^2$;
4. Let $\widehat{\lambda} = \underset{\lambda \in \Lambda}{argmin}\{\widehat{MSE}(\lambda)\}$, and then compute $\widehat{\pi}_0 = \dfrac{\sum_{i=1}^{m} I_{(p_i > \widehat{\lambda})}}{(1-\widehat{\lambda})m}$;
5. Calculate $\widehat{m}_0$ by formula $\widehat{m}_0 = \widehat{\pi}_0 \times m$;
6. Repeat the procedure of Algorithm 2.1.

Because the MHT-B method has higher computational complexity as the number of hypothesis increases, to reduce the computational complexity, Storey et al. [21] proposed the method that selects the optimal λ using the natural cubic spline approach to fit the data points $(\lambda, \widehat{\pi}_0(\lambda))$ where $\lambda \in \Lambda$. And the detail of the multiple hypothesis testing based on the natural cubic spline approach (MHT-NCS) is described as Algorithm 2.5.

Algorithm 2.5 MHT-NCS

Input: The observed p-values $p_1, p_2, \ldots, p_m$ related to the hypotheses $H_1, H_2, \ldots, H_m$, the threshold $\alpha \in (0, 1]$ and the number of hypotheses m.

Output: The corresponding index of $H_{(1)}, H_{(2)}, \ldots, H_{\widehat{(k)}}$.

1. For each given λ from $\Lambda = \{0, 0.05, \ldots, 0.9, 0.95\}$, calculate the corresponding value of $\widehat{\pi}_0(\lambda)$ by the Eq. (5);
2. Obtain the curve $\widehat{f}(\lambda)$ by using the cubic spline with 3 df to fit data points $(\lambda, \widehat{\pi}_0(\lambda))$ where $\lambda \in \Lambda$, and set $\widehat{\pi}_0 = \widehat{f}(1)$;
3. Calculate the $\widehat{m}_0$ by formula $\widehat{m}_0 = \widehat{\pi}_0 \times m$;
4. Repeat the procedure of Algorithm 2.1.

2.3 Multiple Hypothesis Testing Technique Based on the Empirical Bayes Approaches

Consider that the observed p-values $p_1, \ldots, p_m$ come from a mixed distribution, and set $\gamma = 1 - p$, then the density of γ is defined as Eq. (6),

$$f(\gamma) = \pi_0 f_0(\gamma; \theta) + (1 - \pi_0) f_1(\gamma), \tag{6}$$

where θ is some parameters contained in f_0 and π_0 is the true null hypotheses to all null hypotheses ratio. To estimate π_0, Strimmer proposed a unified approach which is a simple semiparametric model using a modified Grenander density estimator and both p values and other statistics can be used to estimate π_0. And the detail of this method can be seen in the literature [22], the corresponding algorithm is implemented in R in the "fdrtool" package and available under the GNU GPL from http://strimmerlab.org/software/fdrtool/. The procedure of the multiple hypothesis testing based on the unified approach (MHT-U) is described in Algorithm 2.6.

Algorithm 2.6 MHT-U

Input: The observed p-values $p_1, p_2, \ldots, p_m$ related to the hypotheses $H_1, H_2, \ldots, H_m$, the threshold $\alpha \in (0, 1]$ and the number of hypotheses m.

Output: The corresponding index of $H_{(1)}, H_{(2)}, \ldots, H_{\widehat{(k)}}$.

1. Estimate π_0 by the algorithm proposed by Strimmer;
2. Calculate $\widehat{m}_0$ by formula $\widehat{m}_0 = \widehat{\pi}_0 \times m$;

3. Repeat the Algorithm 2.1.

Let p_1, p_2,…, p_m denote the observed p-values obtained by m hypotheses test, and then convert the p-values to the z-scores by Eq. (7),

$$z_i = \Phi^{-1}(1 - p_i), \tag{7}$$

where Φ is the standard normal cumulative distribution function. Suppose that the density of z is defined as Eq. (8),

$$f(z) = \pi_0 f_0(z) + (1 - \pi_0) f_1(z), \tag{8}$$

where π_0 is the true null hypotheses to all null hypotheses ratio, and then let $F(z)$ and $F_0(z)$ be the cumulative distribution functions corresponding to the densities $f(z)$ and $f_0(z)$ respectively. Consider a rejection rule $\Lambda = \{z_i \geq z_0\}$, then the conditional expectation of $FDR(z)$ which is called bayesian false discovery rate [28] is defined as Eq. (9), and a natural estimator of $FDR(z)$ which also used in Liang et al. [29] is defined as Eq. (10),

$$FDR(z) = \frac{\pi_0(1 - F_0(z_0))}{1 - F(z_0)}, \tag{9}$$

$$\widehat{FDR}(z) = \frac{m\hat{\pi}_0(1 - \hat{F}_0(z_0))}{\sum_{i=1}^{m} I_{(z_i \geq z_0)}}, \tag{10}$$

where $I_{(\cdot)}$ is an indicator function and z_0 is a given constant. Then, the q-value which is similar to Storey [20] is defined as Eq. (11),

$$q(z) \equiv \inf_{\{\Lambda : z \in \Lambda\}} FDR(\Lambda). \tag{11}$$

To estimate q-values, the method proposed by Liang et al. [15] is to use a mixture of exponential power distribution to model $f(z)$ and estimate the parameters using the stochastic approximation algorithm. To further improve the efficiency of the method, we replace the stochastic approximation algorithm with the Adam algorithm [30] to estimate the parameters. In more detail, we assume that $f(z)$ is formed by a mixture of exponential power distributions as follows:

$$f(z;\theta) = \sum_{i=1}^{N} \omega_i \varphi_i(z;\mu_i,\alpha_i,\beta_i) = \sum_{i=1}^{N} \omega_i \frac{\beta_i}{2\alpha_i \Gamma\left(\frac{1}{\beta_i}\right)} \exp\left\{ -\left(\frac{|z - \mu_i|}{\alpha_i} \right)^{\beta_i} \right\}, \tag{12}$$

where $\theta = (\mu_1, \alpha_1, \beta_1, \ldots, \mu_N, \alpha_N, \beta_N, \omega_1, \ldots, \omega_{N-1})$ is parameters of model; N is the total number of components; $0 < \omega_i \leq 1$ denotes the weight of ith component and $\sum_{i=1}^{N} \omega_i = 1$ holds; and the location parameter $\mu_i \in (-\infty, +\infty)$ represents the centre of the ith exponential power distribution; the scale parameter $\alpha_i \in (0, +\infty)$ represents the dispersion of the ith exponential power distribution; and the shape parameter $\beta_i \in (1, +\infty)$ represents the rate of exponential decay of the ith exponential power distribution. And in order to simplify the calculation, we convert θ as $\theta^* = (\mu_1^*, \alpha_1^*, \beta_1^*, \ldots, \mu_N^*, \alpha_N^*, \beta_N^*, \omega_1^*, \ldots, \omega_{N-1}^*)$, where $\omega_N^* = 0$ and $\omega_i = \exp(\omega_i^*) / \sum_{j=1}^{N} \exp(\omega_j^*)$ holds for all $i = 1, 2, \ldots, N - 1$; and $\mu_i^* \equiv \mu_i$, $\alpha_i^* = \log(\alpha_i)$ and $\beta_i^* = \log(\beta_i - 1)$ hold for all $i = 1, 2, \ldots, N$. Then, we denote $f(z; \theta)$ by $f(z; \theta^*)$ in below. Moreover, the mixture distribution can be estimated by minimizing the Kullback-Leibler (K-L)

distance defined in Eq. (13) when N is given, and because the true density $f(z)$ is unknown, the Adam algorithm can be used to estimate the parameters.

$$KL(f_{\theta^*},f) \equiv -\int \log\left\{\frac{f(z;\theta^*)}{f(z)}\right\} f(z)\,dz. \tag{13}$$

By differentiating $KL(f_{\theta^*}, f)$ with respect to θ^* , we can get the Eqs. (14)–(17),

$$H_{\omega_i^*}(\theta,z) = P(i,z)(1-\omega_i), i = 1,2,\ldots,N-1, \tag{14}$$

$$H_{\mu_i^*}(\theta,z) = P(i,z)\left\{(-1)^{I(z<\mu_i)}\frac{\beta_i}{\alpha_i}\left|\frac{z-\mu_i}{\alpha_i}\right|^{\beta_i-1}\right\}, i = 1,2,\ldots,N, \tag{15}$$

$$H_{\alpha_i^*}(\theta,z) = P(i,z)\left\{-\frac{1}{\alpha_i}+\frac{\beta_i}{\alpha_i}\left(\frac{|z-\mu_i|}{\alpha_i}\right)^{\beta_i}\right\}\alpha_i, i = 1,2,\ldots,N, \tag{16}$$

$$H_{\beta_i^*}(\theta,z) = (\beta_i-1)P(i,z)\left\{\frac{1}{\beta_i}+\frac{\Gamma'(1/\beta_i)}{(\beta_i)^2\Gamma(1/\beta_i)}\right\} - (\beta_i-1)P(i,z)\left\{\left|\frac{z-\mu_i}{\alpha_i}\right|^{\beta_i}\log\left|\frac{z-\mu_i}{\alpha_i}\right|\right\}, \quad i = 1,2,\ldots,N, \tag{17}$$

where $I(\cdot)$ is the indicator function and $P(i,z) = \omega_i\dfrac{\varphi_i(z;\mu_i,\alpha_i,\beta_i)}{f(z;\theta^*)}$, and then we use the Adam algorithm to get the estimator $\hat{\theta}$. Suppose that the components of $f(z;\hat{\theta})$ are ordered such that $\hat{\mu}_1 \le \hat{\mu}_2 \le \cdots \le \hat{\mu}_N$, then the distance between two neighbouring components is defined as:

$$d_{KL}(\widehat{\varphi}_i,\widehat{\varphi}_{i+1}) = \frac{(KL(\widehat{\varphi}_i,\widehat{\varphi}_{i+1}) + KL(\widehat{\varphi}_{i+1},\widehat{\varphi}_i))}{2}, \tag{18}$$

where $\widehat{\varphi}_i$ is the ith component of $f(z;\hat{\theta})$. Because $d_{KL}(\widehat{\varphi}_i,\widehat{\varphi}_{i+1})$ is not analytically available for exponential power distributions, we use Metropolis-Hastings samples simulated from $\widehat{\varphi}_i$ and $\widehat{\varphi}_{i+1}$ to estimate it. Then, the fist N_0 components of $f(z;\hat{\theta})$ are classified into the group f_0 and π_0 is estimated by $\widehat{\pi}_0 = \sum_{i=1}^{N_0}\widehat{\omega}_i$, and N_0 is calculated by Eq. (19). And the procedure of the multiple hypothesis testing based on the Adam approach (MHT-Adam) is described as Algorithm 2.7.

$$N_0 = \arg\min_i d_{KL}(\widehat{\varphi}_i,\widehat{\varphi}_{i+1}). \tag{19}$$

Algorithm 2.7 MHT-Adam

Input: The observed p-values $p_1,p_2,\ldots,p_m$ related to the hypotheses $H_1,H_2,\ldots,H_m$. Initialize θ_0^* and calculate θ_0. Set $\lambda_1 = 0$, $\lambda_2 \in [0,1)$, $lr = 0.02$, $\alpha = 0.05$, $\varepsilon = 10^{-8}$ and $t = 0$. Let $m^0 = (m^0_{\mu_1^*}, m^0_{\alpha_1^*}, m^0_{\beta_1^*},\ldots, m^0_{\mu_N^*}, m^0_{\alpha_N^*}, m^0_{\beta_N^*}, m^0_{\omega_1^*},\ldots, m^0_{\omega_{N-1}^*})$ and $v^0 = (v^0_{\mu_1^*}, v^0_{\alpha_1^*}, v^0_{\beta_1^*},\ldots, v^0_{\mu_N^*}, v^0_{\beta_N^*}, v^0_{\omega_1^*},\ldots, v^0_{\omega_{N-1}^*})$ be zero.

Output: The corresponding index of the rejected null hypotheses among hypotheses $H_{(1)},H_{(2)},\ldots,H_{(m)}$.

1. Calculate the z-scores $(z_1,z_2,\ldots,z_m)$ via Eq. (7);
2. Random select z^t from the data set $(z_1,\ldots,z_m)$ with replacement;
3. Let $t = t+1$ and update $g^t = (g^t_{\mu_1^*}, g^t_{\alpha_1^*}, g^t_{\beta_1^*},\ldots, g^t_{\mu_N^*}, g^t_{\alpha_N^*}, g^t_{\beta_N^*}, g^t_{\omega_1^*},\ldots, g^t_{\omega_{N-1}^*})$ by following formulas;

$$g^t_{\omega^*_i} = H_{\omega^*_i}(\theta_{t-1}, z^{t-1}) \text{ for } i = 1, \ldots, N-1,$$
$$g^t_{\mu^*_i} = H_{\mu^*_i}(\theta_{t-1}, z^{t-1}) \text{ for } i = 1, \ldots, N,$$
$$g^t_{\alpha^*_i} = H_{\alpha^*_i}(\theta_{t-1}, z^{t-1}) \text{ for } i = 1, \ldots, N,$$
$$g^t_{\beta^*_i} = H_{\beta^*_i}(\theta_{t-1}, z^{t-1}) \text{ for } i = 1, \ldots, N.$$

4. Calculate θ^*_t by the following formulas;

$$m^t = \lambda_1 m^{t-1} + (1-\lambda_1) g^t,$$
$$\hat{m}^t = \frac{m^t}{(1-(\lambda_1)^t)},$$
$$v_t = \lambda_2 v^{t-1} + (1-\lambda_2)(g^t)^2,$$
$$\hat{v}^t = \frac{v^t}{(1-(\lambda_2)^t)},$$
$$\theta^*_t = \theta^*_{t-1} + lr \frac{\hat{m}^t}{\left(\sqrt{\hat{v}t} + \varepsilon\right)}.$$

5. Repeat the Steps 2–4 until θ^*_t is converged;
6. Compute $\hat{\theta} = \theta_t$ by the relation between θ and θ^*;
7. Compute N_0 via Eq. (19);
8. Estimate $\hat{\pi}_0$ by formula $\hat{\pi}_0 = \sum_{i=1}^{N_0} \hat{\omega}_i$;
9. Calculate $\widehat{FDR}(\Lambda)$ via Eq. (10);
10. Estimate $\hat{q}(z_i) = \inf_{\{\Lambda: z \in \Lambda\}} \widehat{FDR}(\Lambda)$ for all $i = 1, 2, \ldots, m$;
11. Reject the null hypotheses among $H_{(1)}, H_{(2)}, \ldots, H_{(m)}$ with the corresponding $\hat{q}(z_i)$ less than α, and record the corresponding index of the rejected null hypotheses.

2.4 The Biomarker Selection Approach Based on the Multiple Hypothesis Testing Techniques

Compared with the frequentist methods, the empirical Bayes methods estimate FDR by using an empirical null distribution instead of assuming the null p-values are uniformly distributed. Thus, the biomarker selection approach by combining the results of the frequentist methods and the empirical Bayes methods can reduce the influence of inductive bias and improve the accuracy of the result. The biomarker selection approach based on the multiple hypothesis testing techniques colligates six methods (i.e., MHT-SE, MHT-LSE, MHT-B, MHT-NCS, MHT-U and MHT-Adam), where the MHT-U and MHT-Adam methods belong to the empirical Bayes methods and the rest belongs to the frequentist methods. Based on the biomarker selection approach proposed here, the abnormal brain regions and the abnormal functional connectivity can be identified. In more detail, we run these six methods 30 times each and count the total frequency of each feature with six methods, then the features with higher frequency constitute the optimal subset. The flowchart of the biomarker selection approach based on the multiple hypothesis testing techniques is shown in Fig. 1.

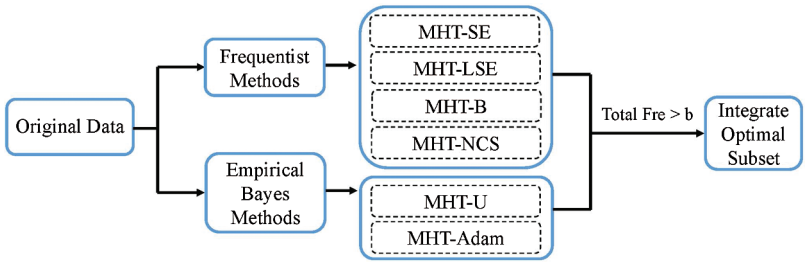

Figure 1: The flowchart of the biomarker selection approach based on the multiple hypothesis testing techniques, where Fre denotes the frequency and b is a given constant

2.5 Network Analysis Based on Graph Theory

In order to show the good performance of the biomarker selection approach and evaluate the difference of the topological properties between the original network and the processed network, we choose four network characteristics as the network evaluation index which can characterize the topological attributes of the network, i.e., clustering coefficient (C), characteristic path length (L), global network efficiency (Eg) and local network efficiency ($Eloc$), and the formula of these network characteristics are shown in Fig. A1. The clustering coefficient reflects the ability of a specialized process to occur within some densely interconnected groups of the brain regions. The characteristic path length reflects the ability to rapidly combine some specialized information from distributed brain regions. The global and local network efficiency reflects the ability to transmit information from the different brain regions of the global network and local network respectively. In more detail, we use the original FNC data and the FNC data processed by the biomarker selection approach to construct the original network and the processed network for each sample respectively, and we calculate the values of the four network characteristics corresponding to these two networks for each sample, then the p-values of the four network characteristics corresponding to these two networks are computed. Based on these p-values, the difference between the original network and the processed network can be found.

3 Results

In this section, the results and analysis of the abnormal brain regions as well as connections are presented by applying the biomarker selection approach based on the multiple hypothesis testing techniques on the MRI data, then the analysis of the brain networks based on the graph theory is implemented to verify the selected abnormal connectivity, and we also compared our approach with the other two methods to show the validity of the method proposed here.

3.1 Data Collection and Preprocessing

The data used in this study are from Machine Learning for Signal Processing (MLSP) 2014 SZ classification challenge (https://www.kaggle.com/c/mlsp-2014-mri), and it was collected on a 3T MRI scanner at the Mind Research Network and funded by the Centers of Biomedical Research Excellence. And the preprocessing process of the data is that, first, all images were preprocessed using statistical parametric mapping software (SPM, http://www.fll.ion.ucl.ac.uk/spm), and then the SBM and FNC features from the structural MRI and resting-state functional MRI were extracted by the GIFT Toolbox (http://mialab.mrn.org/software/gift/).

The data that consists of 46 HCs and 40 SZ has 410 features, i.e., 32 SBM features and 378 FNC features, and the Structured Clinical Interview for DSM-IV (SCID; Diagnostic and Statistical Manual of Mental Disorders, DSM) is used to make a diagnosis of SZ [31]. Among these features, the SBM features which indicate the concentration of gray matter in different brain regions are weights of the brain regions [32], and the FNC features which can be regarded as a functional modality feature describing the overall level of synchronicity between brain areas of subjects are pairwise correlation values between the time-courses of 28 brain regions [33]. And these 28 brain regions selected according to the Automated Anatomical Labeling atlas (AAL) and the connections between 28 brain regions are shown in Figs. A2 and A3.

3.2 Results Based on the Biomarker Selection Approach

Through the Wilcoxon Rank-sum test for each feature of the data, we can get the corresponding p-values and it is the input to the experiment. Then the total frequency of each feature is obtained by applying the biomarker selection approach based on the multiple hypothesis testing techniques, and the results are shown in Figs. 2 and 3. It is widely accepted that the importance of feature is related to frequency, i.e.,

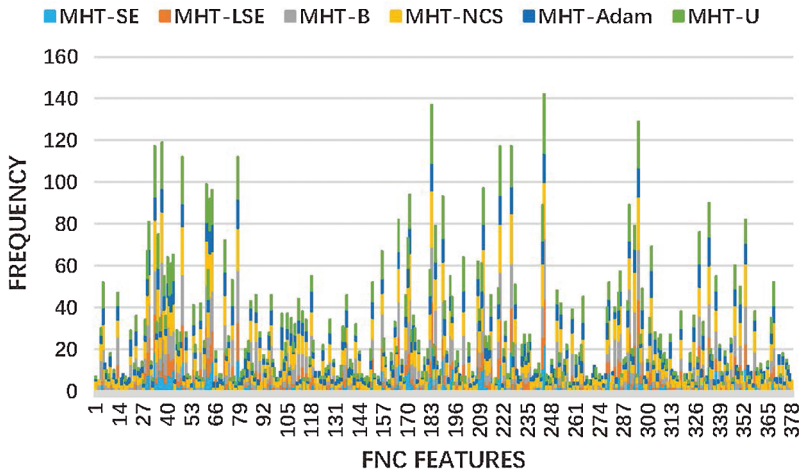

Figure 2: The frequency of FNC features by the biomarker selection approach based on the multiple hypothesis testing techniques

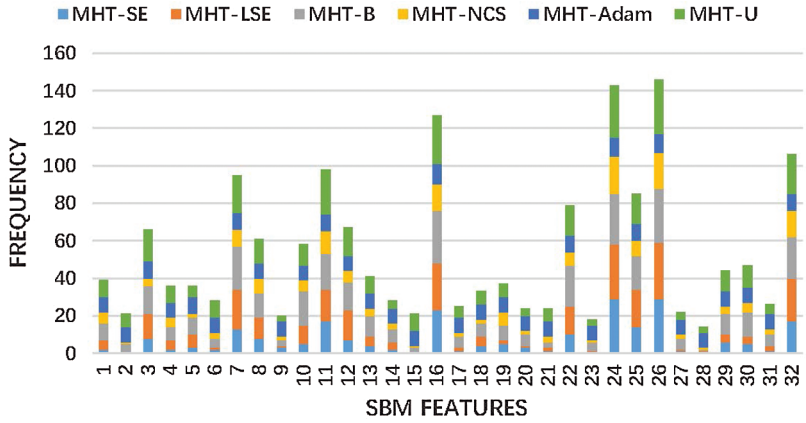

Figure 3: The frequency of SBM features by the biomarker selection approach based on the multiple hypothesis testing techniques

the frequency of feature is too low, then it is believed that this feature is not important. Therefore we set a threshold b to filter the unimportant features, i.e., the features with a frequency lower than b are removed, and the remaining features are selected as the biomarkers. Besides, the threshold b can be decided by the elbow criterion which is to find a knee point from the feature frequency distribution curve. In the coordinate systems that the abscissa is the frequency of occurrence and the ordinate is the number of features, the feature frequency distribution curve is drawn, and the point (x,y) in the coordinate systems represents that the number of features with the frequency of occurrence greater than or equal to x is y. And the knee point should balance the number of features and the frequency of occurrence. Thus we select the significant SBM features by intercepting high frequency greater than 95 and select frequency greater than 79 as the significant FNC features. By intercepting high frequencies, we find that there are six significant SBM features with index 7, 11, 16, 24, 26 and 32, and there are 23 significant FNC features with index 30, 33, 37, 48, 61, 63, 64, 78, 165, 171, 183, 185, 189, 211, 220, 226, 243, 244, 290, 293, 295, 333 and 353. Moreover, we show the location of the abnormal brain regions and connectivity in Figs. 4 and 5.

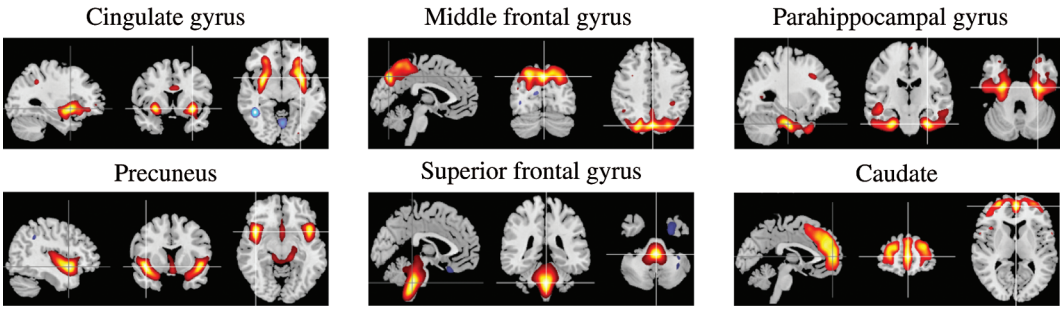

Figure 4: The aberrant brain regions of SZ by the biomarker selection approach based on the multiple hypothesis testing techniques

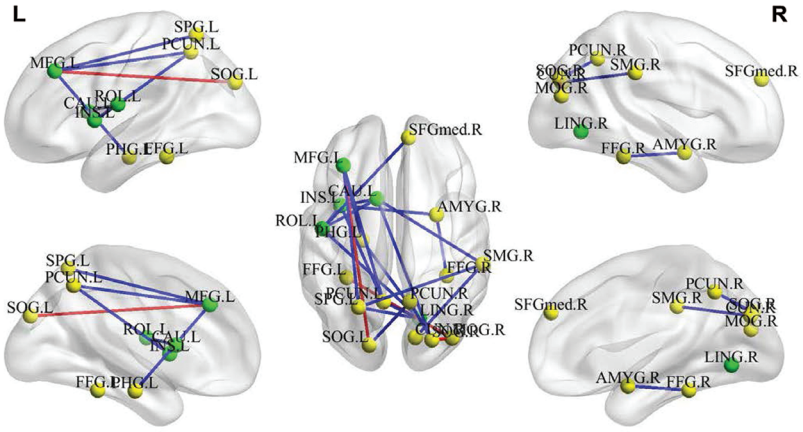

Figure 5: The abnormal functional connections of SZ by the biomarker selection approach based on the multiple hypothesis testing techniques. The five regions with the most connections are marked by the green node, and the rest regions are marked by the yellow node. The red and blue edge denotes that, compared with HCs, the connection of two regions is strengthened and reduced in SZ respectively

Fig. 4 shows the six aberrant brain regions of SZ. These regions are located in the cingulate gyrus (CG), middle frontal gyrus (MFG), parahippocampal gyrus (PHG), precuneus (PCUN), superior frontal gyrus (SFG) and caudate (CAU). Among these aberrant brain regions, the significantly reduced gray matter volumes (GMV) are CG, PHG, PCUN and CAU, and the significantly increased GMV lies in frontal gyrus namely MFG and SFG.

Fig. 5 displays the 23 abnormal functional connections of SZ, of which there are five regions with the most connections namely rolandic operculum (ROL), middle frontal gyrus (MFG), insula (INS), lingual gyrus (LING) and caudate nucleus (CAU). In the five regions with the most connections, connecting to ROL are superior frontal gyrus, insula, lingual gyrus and caudate nucleus; connecting to MFG are precuneus, parahippocampal gyrus, superior parietal gyrus and superior occipital gyrus; connecting to INS are rolandic operculum, precuneus, caudate nucleus and amygdala; connecting to LING are rolandic operculum, precuneus, parahippocampal gyrus and superior parietal gyrus and connecting to CAU are rolandic operculum, insula, supramarginal gyrus and superior occipital gyrus. Among the 23 abnormal connectivity discovered by us, only three connections are significantly increased namely the connection of the MFG and the superior occipital gyrus, the connection of the superior occipital gyrus and the middle occipital gyrus, the connection of the middle occipital gyrus and the fusiform gyrus, and the rest connections are reduced.

3.3 Comparison with Network Analysis and Other Methods

To find the difference between the original network and the processed network, we use the GRETNA toolbox [34] to compute the four network characteristics of each network. Then, we use the two-sample-*t*-test to test the four network characteristics between HCs and SZ for these two networks. The results of the network analysis are shown in Fig. 6, and the *p*-values corresponding to the four network characteristics for the original network are 1.70×10^{-1}, 5.02×10^{-3}, 2.99×10^{-2}, 4.27×10^{-2}, and the *p*-values corresponding to the four network characteristics for the processed network are 1.49×10^{-2}, 6.02×10^{-7}, 2.20×10^{-9}, 6.56×10^{-3}. It is obvious that all the *p*-values of the four network characteristics significantly reduce after the processing by the biomarker selection approach, which suggests that the HCs group and SZ group become more distinguishable after the processing by the biomarker selection approach and testifies that the biomarker selection approach proposed here is valid to select the biomarkers in SZ. Moreover, it can be seen that only *L* goes up obviously, and all three other network characteristics of SZ goes down evidently compared with HCs, especially the *Eg*. And it reflects that the ability to transmit information from diverse brain regions, the ability of a specialized process to occur within some densely interconnected groups of the brain regions and the ability to rapidly combine some specialized information from distributed brain regions in SZ are lower than HCs. In summary, the noticeable changes of the four network characteristics after the processing by the biomarker selection approach suggest that the ability to integrate and transmit information from distributed brain regions significantly decline in SZ, and confirm that the method proposed here is effective to identify the biomarkers in SZ.

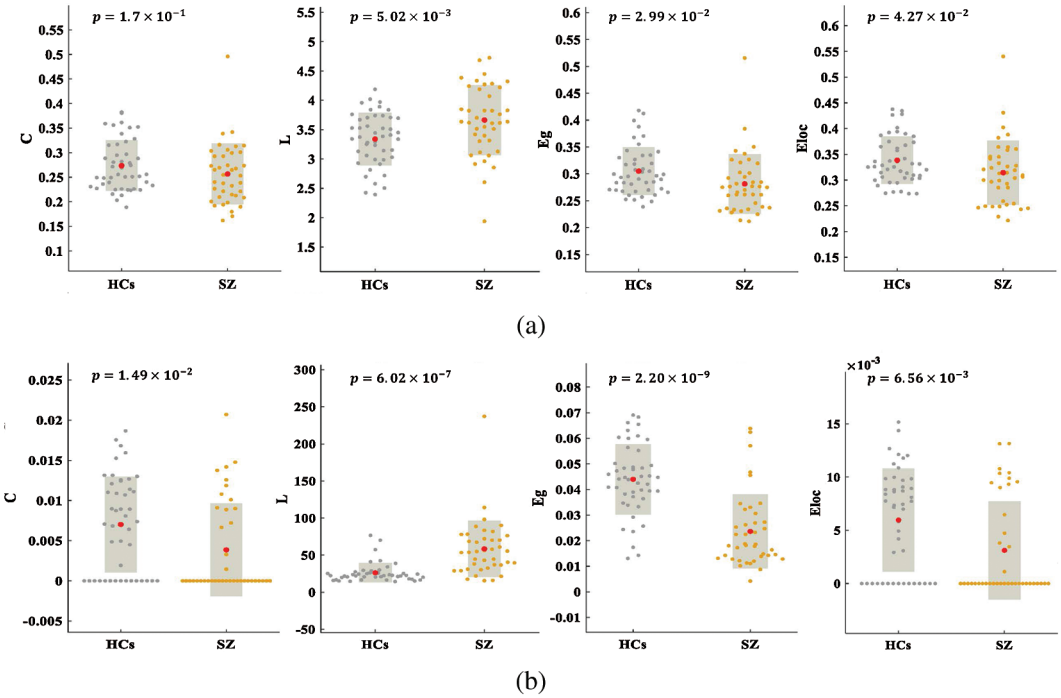

Figure 6: (a) The statistical differences of the four network characteristics between the HCs group and the SZ group before the data processing by the biomarker selection approach. (b) The statistical differences of the four network characteristics between the HCs group and the SZ group after the data processing by the biomarker selection approach

To show the validity of the method proposed here, we compared our approach with the other two methods, i.e., Network-Based Statistics method (NBS) [4] and Multi-Link Analysis method (MLA) [7], where NBS performs univariate *t*-tests among the features while MLA performs a sparse multivariate regression. Because the NBS method can only process the FNC data, we can obtain seven significant FNC features with index 33, 37, 48, 183, 220, 244 and 295 by implementing the NBS method to the FNC data. The significant feature set selected by the NBS method are subset of our significant feature set, and it indicates that our approach is effective to identify the significant features. In addition, the results by implementing the MLA method to the FNC and SBM data are shown in Fig. A4, and there are 50 features out of 410 features with occurrence equal to 40 are selected as significant features. The significant FNC features with index 33, 165, 189, 220, 243, 353 and the significant SBM features with index 7, 11, 24, 26 which selected by the MLA method are also selected by our approach. Moreover, most of the significant features selected by our approach also have the higher occurrence in the MLA method. Compared with the NBS and MLA methods, our approach is more robust by combining six methods, and it also can reduce the influence of inductive bias and improve the accuracy of the result.

4 Discussion

In our findings, there are six abnormal regions. Among these six regions, CG, MFG and PCUN belong to the default mode network (DMN) that was first proposed by Raichle et al. [35] and describes the areas of the brain that are more active during a state of awake but not actively goal-directed behavior, and the regions that comprise the DMN are involved in the integration of autobiographic, self-monitoring, and social cognitive functions [36]. Moreover, it is reported that SZ had lower functional connectivity strength in the PCUN with the rest regions of the DMN compared with HCs [37]. Du et al. [38] find that SZ show impaired interaction among DMN subsystems, and they suggested that decreased integration of DMN may be associated with impaired ability in making self-other distinctions and coordinating present mental states with episodic decisions about future for SZ. The significant reduction of GMV mainly distribute in the regions of CG, PHG, PCUN and CAU, where CG and PHG belong to the limbic lobe and CAU belongs to the basal ganglia. The PHG is related to memory impairments and affective dysregulation, and the CG is related to attention, executive control and emotion generation [39]. Moreover, some results [40,41] are consistent with our results of the GMV decrease in CG and PHG, and suggest that the GMV decrease is involved in auditory verbal hallucinations and violent behavior of SZ. The PCUN plays an important role in many tasks including visuo-spatial imagery, episodic memory retrieval and self-processing operations [42], and the GMV reduction in PCUN is associated with the increased vulnerability to psychosis [24]. Given that CAU is associated with cognitive function and memory ability, the decreased GMV of CAU may have a correlation with the falling memory and cognitive impairment [43].

Not only GMV reduction in SZ, but we also find GMV increase in the SFG and MFG. The dorsolateral prefrontal cortex (DLPFC) including SFG and MFG is crucial in studies of schizophrenia and working memory [44]. Although there is literature to show the GMV decrease of frontal gyrus in SZ [45], evidence also suggests the GMV increase in frontal gyrus [46]. And the different results may be caused by distinct methodology or data. Even the change of GMV of frontal gyrus is not clear, it is undeniable that the abnormality of frontal gyrus has a correlation with schizophrenia [44].

Among the 23 abnormal connectivity, the five regions with the most connections are ROL, MFG, INS, LING and CAU, and most connections are reduced. ROL which is participating in the language production and other verbal functionalities lies at the lower region of the postcentral gyrus [47]. It is reported that the lesions of ROL are related to articulatory disorders which are a component of speech production [25]. Moreover, it is also reported that SZ is relevant to the abnormal connections of ROL and the abnormity of ROL may explain the clinical symptom of SZ that SZ goes short of the content of speech [48]. INS is considered as a limbic region and plays a key role in the high-level cognitive control and attentional

processes. Meanwhile, as the integral hub of the salience network, INS plays a vital function in process of salience network assisting target brain regions in generating appropriate behavioral responses to saliency stimuli [49]. Thus it shows that the decreased connections of INS may result in the dysfunction of the salience network and cognitive deficit in SZ. LING on the medial surface of the occipital lobe lies just below the calcarine fissure [50], which is reported that the strength of the connections of LING is reduced and the reason for the decrease is a disruption of short-range regional functional connectivity strength [51].

Although it is generally considered that most of the connections are decreased in SZ, some studies also found that there are increased connections in SZ [52]. And except the decreased connections, three enhanced connections among 23 abnormal connectivity are also discovered, i.e., the connection of MFG and superior occipital gyrus, the connection of superior occipital gyrus and Middle occipital gyrus, the connection of middle occipital gyrus and fusiform gyrus. According to the report that some regions are activated in the implicit memory retrieval with unpleasant words in SZ, such as fusiform gyrus, occipital gyrus and etc. [53]. Therefore the enhanced connections of occipital gyrus have the potential to illustrate the neural mechanisms corresponding negative emotion in SZ, and which suggests that we do find the aberrant brain regions and connectivity mainly related to cognitive impairment and negative emotion in SZ. Besides, the results may help us to further understand the causes of SZ and also can be used as biomarkers for the diagnosis of mental disorders.

The results are obtained by the biomarker selection approach which combines the six multiple hypothesis testing methods, and from Figs. 2 and 3, the SBM feature with index 11 (i.e., MFG) is not selected by the MHT-LSE, MHT-B as well as MHT-Adam methods and the FNC feature with index 63 (i.e., the connectivity of MFG and PHG) is not selected by the MHT-SE method. However, these two features which are related to SZ reported by some studies [46,54,55] are selected as significant features by the biomarker selection approach. Thus, it shows that the biomarker selection approach can find the important biomarkers in SZ which are discarded by a single method. Moreover, compared with the NBS and MLA methods, our approach is more robust and also can identify the biomarkers which are basically consistent with the previous research. In this paper, the data we used is based on the AAL atlas that is usually able to reflect the functional organization of brain due to a certain correlation between brain functions and its anatomy [56]. It is one of the most frequently used atlas in functional connectivity studies, while some studies consider that AAL atlas had the lower homogeneity of all parcellations and was not the best selection for functional connectivity analysis [57]. In the future study, we will try other better atlas for functional connectivity analysis.

5 Conclusion

By applying the approach proposed here, we find six aberrant brain regions and 23 abnormal connectivity in SZ, of which the significantly reduced GMV are mainly distributed in the limbic lobe and basal ganglia; the significantly increased GMV are distributed in frontal gyrus; the significantly strengthen connections are the connection of MFG and superior occipital gyrus, the connection of superior and middle occipital gyrus as well as the connection of middle occipital gyrus and fusiform gyrus; and the rest connections are significantly weakened. It is reported that these abnormal brain regions and connectivity are strongly related to auditory verbal hallucinations, violent behavior, falling memory, cognitive impairment, speech disorder, negative emotion and the abnormal of the salience network in SZ. Thus the study of the abnormal brain regions and connectivity in SZ is important for revealing the abnormal neural mechanism of the brain disease, the accurate location of the brain abnormal regions and abnormal brain functional connections in SZ can serve for the accurate medical treatment of the disease and not only improve the accurate diagnosis ability of the brain disease but also guide the clinical intervention and treatment.

Funding Statement: This work was supported by NSFC (No. 11471006 and No. 81601456), Science and Technology Innovation Plan of Xi'an (No. 2019421315KYPT004JC006) and the HPC Platform, Xi'an Jiaotong University.

Conflicts of Interest: The authors declare no conflicts of interest to report regarding the present study.

References

1. Marín, O. (2012). Interneuron dysfunction in psychiatric disorders. *Nature Reviews Neuroscience, 13(2),* 107–120. DOI 10.1038/nrn3155.
2. Sui, J., Qi, S., van Erp, T. G. M., Bustillo, J., Jiang, R. et al. (2018). Multimodal neuromarkers in schizophrenia via cognition-guided MRI fusion. *Nature Communications, 9(1),* 3028. DOI 10.1038/s41467-018-05432-w.
3. van den Heuvel, M. P., Fornito, A. (2014). Brain networks in schizophrenia. *Neuropsychology Review, 24(1),* 32–48. DOI 10.1007/s11065-014-9248-7.
4. Zalesky, A., Fornito, A., Seal, M. L., Cocchi, L., Westin, C. F. et al. (2011). Disrupted axonal fiber connectivity in schizophrenia. *Biological Psychiatry, 69(1),* 80–89. DOI 10.1016/j.biopsych.2010.08.022.
5. Chang, M., Womer, F. Y., Edmiston, E. K., Bai, C., Zhou, Q. et al. (2018). Neurobiological commonalities and distinctions among three major psychiatric diagnostic categories: a structural MRI study. *Schizophrenia Bulletin, 44(1),* 65–74. DOI 10.1093/schbul/sbx028.
6. Du, Y., Fryer, S. L., Lin, D., Sui, J., Yu, Q. et al. (2017). Identifying functional network changing patterns in individuals at clinical high-risk for psychosis and patients with early illness schizophrenia: a group ICA study. *NeuroImage: Clinical, 17,* 335–346. DOI 10.1016/j.nicl.2017.10.018.
7. Crimi, A., Giancardo, L., Sambataro, F., Gozzi, A., Murino, V. et al. (2018). Multi-link analysis: brain network comparison via sparse connectivity analysis. https://www.biorxiv.org/content/early/2018/03/08/277046.
8. Suk, H. I., Lee, S. W., Shen, D. (2017). Deep ensemble learning of sparse regression models for brain disease diagnosis. *Medical Image Analysis, 37,* 101–113. DOI 10.1016/j.media.2017.01.008.
9. Demirhan, A. (2018). The effect of feature selection on multivariate pattern analysis of structural brain MR images. *Physica Medica, 47,* 103–111. DOI 10.1016/j.ejmp.2018.03.002.
10. Cao, F., Liu, Y., Wang, D. (2018). Efficient saliency detection using convolutional neural networks with feature selection. *Information Sciences, 456,* 34–49. DOI 10.1016/j.ins.2018.05.006.
11. Liu, Z., Wu, M., Cao, W., Mao, J., Xu, J. et al. (2018). Speech emotion recognition based on feature selection and extreme learning machine decision tree. *Neurocomputing, 273(1),* 271–280. DOI 10.1016/j.neucom.2017.07.050.
12. Qiao, C., Lu, L., Yang, L., Kennedy, P. J. (2019). Identifying brain abnormalities with schizophrenia based on a hybrid feature selection technology. *Applied Sciences, 9(10),* 2148. DOI 10.3390/app9102148.
13. George, E. I. (2000). The variable selection problem. *Journal of the American Statistical Association, 95(452),* 1304–1308. DOI 10.1080/01621459.2000.10474336.
14. Kirkham, E. M., Weaver, E. M. (2015). A review of multiple hypothesis testing in otolaryngology literature. *Laryngoscope, 125(3),* 599–603. DOI 10.1002/lary.24857.
15. Liang, F., Zhang, J. (2008). Estimating the false discovery rate using the stochastic approximation algorithm. *Biometrika, 95(4),* 961–977. DOI 10.1093/biomet/asn036.
16. Hochberg, Y., Benjamini, Y. (1990). More powerful procedures for multiple significance testing. *Statistics in Medicine, 9(7),* 811–818. DOI 10.1002/sim.4780090710.
17. Schweder, T., Spjøtvoll, E. (1982). Plots of *p*-values to evaluate many tests simultaneously. *Biometrika, 69(3),* 493–502. DOI 10.1093/biomet/69.3.493.
18. Benjamini, Y., Hochberg, Y. (1995). Controlling the false discovery rate: a practical and powerful approach to multiple testing. *Journal of the Royal Statistical Society. Series B (Methodological), 57(1),* 289–300. DOI 10.1111/j.2517-6161.1995.tb02031.x.
19. Benjamini, Y., Hochberg, Y. (2000). On the adaptive control of the false discovery rate in multiple testing with independent statistics. *Journal of Educational and Behavioral Statistics, 25(1),* 60–83. DOI 10.3102/10769986025001060.

20. Storey, J. (2002). A direct approach to false discovery rates. *Journal of the Royal Statistical Society. Series B: Statistical Methodology, 64(3),* 479–498. DOI 10.1111/1467-9868.00346.
21. Storey, J. D., Tibshirani, R. (2011). Statistical significance for genomewide studies. *Proceedings of the National Academy of Sciences, 100(16),* 9440–9445. DOI 10.1073/pnas.1530509100.
22. Strimmer, K. (2008). A unified approach to false discovery rate estimation. *BMC Bioinformatics, 9(1),* 303. DOI 10.1186/1471-2105-9-303.
23. Mennigen, E., Miller, R. L., Rashid, B., Fryer, S. L., Loewy, R. L. et al. (2018). Reduced higher-dimensional resting state fMRI dynamism in clinical high-risk individuals for schizophrenia identified by meta-state analysis. *Schizophrenia Research, 201,* 217–223. DOI 10.1016/j.schres.2018.06.007.
24. Borgwardt, S. J., Riecher-Rössler, A., Dazzan, P., Chitnis, X., Aston, J. et al. (2007). Regional gray matter volume abnormalities in the at risk mental state. *Biological Psychiatry, 61(10),* 1148–1156. DOI 10.1016/j.biopsych.2006.08.009.
25. Tonkonogy, J., Goodglass, H. (1981). Language function, foot of the third frontal gyrus, and rolandic operculum. *Archives of Neurology, 38(8),* 486–490. DOI 10.1001/archneur.1981.00510080048005.
26. Neyman, J., Pearson, E. S. (1933). On the problem of the most efficient tests of statistical hypotheses. *Philosophical Transactions of the Royal Society of London. Series A, Containing Papers of a Mathematical or Physical Character, 231,* 289–337. http://www.jstor.org/stable/91247.
27. Farcomeni, A. (2008). A review of modern multiple hypothesis testing, with particular attention to the false discovery proportion. *Statistical Methods in Medical Research, 17(4),* 347–388. DOI 10.1177/0962280206079046.
28. Efron, B. (2004). Large-scale simultaneous hypothesis testing. *Journal of the American Statistical Association, 99 (465),* 96–104. DOI 10.1198/016214504000000089.
29. Liang, F., Liu, C., Wang, N. (2007). A robust sequential Bayesian method for identification of differentially expressed genes. *Statistica Sinica, 17(2),* 571–597. https://statistica/j17n2/j17n28/j17n28.html.
30. Kingma, D., Ba, J. (2014). Adam: a method for stochastic optimization. http://arxiv.org/abs/1412.6980v8.
31. Mittal, V. A., Walker, E. F. (2011). Diagnostic and statistical manual of mental disorders. *Psychiatry Research, 189 (1),* 158–159. DOI 10.1016/j.psychres.2011.06.006.
32. Segall, J., Allen, E., Jung, R., Erhardt, E., Arja, S. et al. (2012). Correspondence between structure and function in the human brain at rest. *Frontiers in Neuroinformatics, 6,* 10. DOI 10.3389/fninf.2012.00010.
33. Allen, E. A., Erhardt, E. B., Damaraju, E., Gruner, W., Segall, J. M. et al. (2011). A baseline for the multivariate comparison of resting-state networks. *Frontiers in Systems Neuroscience, 5,* 2.
34. Wang, J., Wang, X., Xia, M., Liao, X., Evans, A. et al. (2015). Corrigendum: Gretna: a graph theoretical network analysis toolbox for imaging connectomics. *Frontiers in Human Neuroscience, 9,* 458. https://www.frontiersin.org/article/10.3389/fnhum.2015.00458.
35. Raichle, M. E., MacLeod, A. M., Snyder, A. Z., Powers, W. J., Gusnard, D. A. et al. (2001). A default mode of brain function. *Proceedings of the National Academy of Sciences of the United States of America, 98(2),* 676–682. DOI 10.1073/pnas.98.2.676.
36. Leng, X., Xiang, J., Yang, Y., Yu, T., Qi, X. et al. (2020). Frequency-specific changes in the default mode network in patients with cingulate gyrus epilepsy. *Human Brain Mapping, 41(9),* 2447–2459. DOI 10.1002/hbm.24956.
37. Zong, X., Hu, M., Pantazatos, S. P., Mann, J. J., Wang, G. et al. (2018). A dissociation in effects of risperidone monotherapy on functional and anatomical connectivity within the default mode network. *Schizophrenia Bulletin, 45(6),* 1309–1318. DOI 10.1093/schbul/sby175.
38. Du, Y., Pearlson, G. D., Yu, Q., He, H., Lin, D. et al. (2016). Interaction among subsystems within default mode network diminished in schizophrenia patients: a dynamic connectivity approach. *Schizophrenia Research, 170(1),* 55–65. DOI 10.1016/j.schres.2015.11.021.
39. Sturm, V. E., Haase, C. M., Levenson, R. W. (2016). Chapter 22—emotional dysfunction in psychopathology and neuropathology: neural and genetic pathways. In: Lehner, T., Miller, B. L., State, M. W. (eds.). *Genomics, Circuits, and Pathways in Clinical Neuropsychiatry.* San Diego: Academic Press, 345–364. http://www.sciencedirect.com/science/article/pii/B9780128001059000226.

40. Wu, H., Wu, F., Ke, X., Li, R., Lu, X. et al. (2017). Reduced gray matter volume of left superior temporal gyrus in schizophrenia with auditory verbal hallucinations: a voxel-based morphometry study. *BIO Web of Conferences, 8,* 01031. DOI 10.1051/bioconf/20170801031.
41. Yang, Y., Raine, A., Han, C. B., Schug, R. A., Toga, A. W. et al. (2010). Reduced hippocampal and parahippocampal volumes in murderers with schizophrenia. *Psychiatry Research: Neuroimaging, 182(1),* 9–13. DOI 10.1016/j.pscychresns.2009.10.013.
42. Cavanna, A. E., Trimble, M. R. (2006). The precuneus: a review of its functional anatomy and behavioural correlates. *Brain, 129(3),* 564–583. DOI 10.1093/brain/awl004.
43. Trimble, M. (2002). Molecular neuropharmacology, a foundation for clinical neuroscience. *Journal of Neurology, Neurosurgery & Psychiatry, 73(2),* 210. DOI 10.1136/jnnp.73.2.210-a.
44. Weinberger, D. R., Berman, K. F., Zec, R. F. (1986). Physiologic dysfunction of dorsolateral prefrontal cortex in schizophrenia: I—regional cerebral blood flow evidence. *Archives of General Psychiatry, 43(2),* 114–124. DOI 10.1001/archpsyc.1986.01800020020004.
45. Kikinis, Z., Fallon, J., Niznikiewicz, M., Nestor, P., Davidson, C. et al. (2010). Gray matter volume reduction in rostral middle frontal gyrus in patients with chronic schizophrenia. *Schizophrenia Research, 123(2),* 153–159. DOI 10.1016/j.schres.2010.07.027.
46. Chang, M., Womer, F. Y., Bai, C., Zhou, Q., Wei, S. et al. (2016). Voxel-based morphometry in individuals at genetic high risk for schizophrenia and patients with schizophrenia during their first episode of psychosis. *PLoS One, 11(10),* e0163749. DOI 10.1371/journal.pone.0163749.
47. Ferro, A., Roiz-Santiánez, R., Ortíz-García de la Foz, V., Ayesa-Arriola, R., Tordesillas-Gutiérrez, D. et al. (2014): Epa-0799—postcentral gyrus in patients at first episode of schizophrenia: a longitudinal structural mri study. *European Psychiatry, 29,* 1. http://www.sciencedirect.com/science/article/pii/S0924933814781428.
48. GeethaRamani, R., Sivaselvi, K. (2014). Data mining technique for identification of diagnostic biomarker to predict schizophrenia disorder. *IEEE International Conference on Computational Intelligence and Computing Research,* Coimbatore, India.
49. Menon, V., Uddin, L. Q. (2010). Saliency, switching, attention and control: a network model of insula function. *Brain Structure and Function, 214(5),* 655–667. DOI 10.1007/s00429-010-0262-0.
50. Mendoza, E. (2017). Lingual gyrus. In: Kreutzer, J., DeLuca, J., Caplan, B. (eds.). *Encyclopedia of clinical neuropsychology*. Cham: Springer International Publishing.
51. Wang, X., Xia, M., Lai, Y., Dai, Z., Cao, Q. et al. (2014). Disrupted resting-state functional connectivity in minimally treated chronic schizophrenia. *Schizophrenia Research, 156(2),* 150–156. DOI 10.1016/j.schres.2014.03.033.
52. Yu, Q., Allen, E. A., Sui, J., Arbabshirani, M. R., Pearlson, G. et al. (2012). Brain connectivity networks in schizophrenia underlying resting state functional magnetic resonance imaging. *Current Topics in Medicinal Chemistry, 12(21),* 2415–2425. DOI 10.2174/156802612805289890.
53. Kim, G. W., Yang, J. C., Jeong, G. W. (2015). Emotional effect on cognitive control in implicit memory tasks in patients with schizophrenia. *NeuroReport, 26(11),* 647–655. DOI 10.1097/WNR.0000000000000405.
54. Diederen, K. M., Neggers, S. F., Daalman, K., Blom, J. D., Goekoop, R. et al. (2010). Deactivation of the parahippocampal gyrus preceding auditory hallucinations in schizophrenia. *American Journal of Psychiatry, 167(4),* 427–435. DOI 10.1176/appi.ajp.2009.09040456.
55. Escartí, M. J., de la Iglesia-Vayá, M., Martí-Bonmatí, L., Robles, M., Carbonell, J. et al. (2010). Increased amygdala and parahippocampal gyrus activation in schizophrenic patients with auditory hallucinations: an fMRI study using independent component analysis. *Schizophrenia Research, 117(1),* 31–41. DOI 10.1016/j.schres.2009.12.028.
56. Tzourio-Mazoyer, N., Landeau, B., Papathanassiou, D., Crivello, F., Etard, O. et al. (2002). Automated anatomical labeling of activations in SPM using a macroscopic anatomical parcellation of the MNI MRI single-subject brain. *NeuroImage, 15(1),* 273–289. DOI 10.1006/nimg.2001.0978.
57. Gordon, E. M., Laumann, T. O., Adeyemo, B., Huckins, J. F., Kelley, W. M. et al. (2014). Generation and evaluation of a cortical area parcellation from resting-state correlations. *Cerebral Cortex, 26(1),* 288–303. DOI 10.1093/cercor/bhu239.

Appendix A.

Clustering coefficient (C): Average nodal clustering coefficient.	$C=\frac{1}{n}\sum_{i\in N}C_i=\frac{1}{n}\sum_{i\in N}\frac{2t_i}{k_i(k_i-1)}$
Characteristic path length (L): integration and global routing efficiency of a network	$\frac{1}{L}=\frac{1}{n(n-1)}\sum_{i\neq j\in N}\frac{1}{d_{ij}}=\boldsymbol{E_{global}}$
Gamma (γ): the normalized clustering coefficient	$\gamma=C/C_{rand}$
Lambda (λ): the normalized characteristic path length	$\lambda=L/L_{rand}$
Sigma (σ): the extent of small-world property	$\boldsymbol{\sigma=\gamma/\lambda}$
Degree: number of links connected directly to a node	$k_i=\sum_{j\in N}a_{ij}\ / k_i=\sum_{j\in N}w_{ij}$
Nodal clustering coefficient: local clustering and closeness of neighborhood of node	C_i
Nodal efficiency: efficiency for a node communicating with the other	$e_i=\frac{1}{n-1}\sum\nolimits_{j\in N,j\neq i}\frac{1}{d_{ij}}$
Betweenness centrality: a centrality measure in the communications between other nodes	$b_i=\frac{1}{(n-1)(n-2)}\sum_{j\neq i\neq k}\frac{\sigma_{jk}(i)}{\sigma_{jk}}$

Figure A1: Different measuring parameters of the global and local network properties. where t_i is the number of triangles around node i, d_{ij} is the shortest path length between node i and node j, C_{rand} and L_{rand} refer to the average clustering coefficient and characteristic path length values obtained from 100 random networks with the same number of nodes as well as edges and the same degree of distribution as the original network, and σ_{jk} is the number of shortest paths between j and k, and $\sigma_{jk}(i)$ is the number of shortest paths between j and k that pass through i

Labels	*Regions*	*abbr.*	*x(mm)*	*y(mm)*	*z(mm)*
21	Olfactory cortex	OLF.L	-8.06	15.05	-11.46
17	Rolandic operculum	ROL.L	-47.16	-8.48	13.95
7	Middle frontal gyrus	MFG.L	-33.43	32.73	35.46
23	Superior frontal gyrus, medial	SFGmed.L	-4.8	49.17	30.89
24	Superior frontal gyrus, medial	SFGmed.R	9.1	50.84	30.22
38	Hippocampus	HIP.R	29.23	-19.78	-10.33
56	Fusiform gyrus	FFG.R	33.97	-39.1	-20.18
29	Insula	INS.L	-35.13	6.65	3.44
46	Cuneus	CUN.R	13.51	-79.36	28.23
64	Supramarginal gyrus	SMG.R	57.61	-31.5	34.48
67	Precuneus	PCUN.L	-7.24	-56.07	48.01
48	Lingual gyrus	LING.R	16.29	-66.93	-3.87
39	Parahippocampal gyrus	PHG.L	-21.17	-15.95	-20.7
59	Superior parietal gyrus	SPG.L	-23.45	-59.56	58.96
50	Superior occipital gyrus	SOG.R	24.29	-80.85	30.59
53	Inferior occipital gyrus	IOG.L	-36.36	-78.29	-7.84
25	Superior frontal gyrus, medial orbital	ORBsupmed.L	-5.17	54.06	-7.4
68	Precuneus	PCUN.R	9.98	-56.05	43.77
34	Median cingulate and paracingulate gyri	DCG.R	8.02	-8.83	39.79
60	Superior parietal gyrus	SPG.R	26.11	-59.18	62.06
52	Middle occipital gyrus	MOG.R	37.39	-79.7	19.42
72	Caudate nucleus	CAU.R	14.84	12.07	9.42
71	Caudate nucleus	CAU.L	-11.46	11	9.24
55	Fusiform gyrus	FFG.L	-31.16	-40.3	-20.23
42	Amygdala	AMYG.R	27.32	0.64	-17.5
20	Supplementary motor area	SMA.R	8.62	0.17	61.85
47	Lingual gyrus	LING.L	-14.62	-67.56	-4.63
49	Superior occipital gyrus	SOG.L	-16.54	-84.26	28.17

Figure A2: 28 brain regions selected for the experiment according to the AAL atlas

Fea	R1	R2	Fea	R1	R2	Fea	R1	R2	Fea	R1	R2	Fea	R1	R2	Fea	R1	R2	Fea	R1	R2
1	21	17	49	17	55	97	23	71	145	38	20	193	46	59	241	67	47	289	50	25	337	34	71
2	21	7	50	17	42	98	23	55	146	38	47	194	46	50	242	67	49	290	50	68	338	34	55
3	21	23	51	17	20	99	23	42	147	38	49	195	46	53	243	48	39	291	50	34	339	34	42
4	21	24	52	17	47	100	23	20	148	56	29	196	46	25	244	48	59	29 2	50	60	340	34	20
5	21	38	53	17	49	101	23	47	149	56	46	197	46	68	245	48	50	293	50	52	341	34	47
6	21	56	54	7	23	102	23	49	150	56	64	198	46	34	246	48	53	294	50	72	342	34	49
7	21	29	55	7	24	103	24	38	151	56	67	199	46	60	247	48	25	295	50	71	343	60	52
8	21	46	56	7	38	104	24	56	152	56	48	200	46	52	248	48	68	296	50	55	344	60	72
9	21	64	57	7	56	105	24	29	153	56	39	201	46	72	249	48	34	297	50	42	345	60	71
10	21	67	58	7	29	106	24	46	154	56	59	202	46	71	250	48	60	298	50	20	346	60	55
11	21	48	59	7	46	107	24	64	155	56	50	203	46	55	251	48	52	299	50	47	347	60	42
12	21	39	60	7	64	108	24	67	156	56	53	204	46	42	252	48	72	300	50	49	348	60	20
13	21	59	61	7	67	109	24	48	157	56	25	205	46	20	253	48	71	301	53	25	349	60	47
14	21	50	62	7	48	110	24	39	158	56	68	206	46	47	254	48	55	302	53	68	350	60	49
15	21	53	63	7	39	111	24	59	159	56	34	207	46	49	255	48	42	303	53	34	351	52	72
16	21	25	64	7	59	112	24	50	160	56	60	208	64	67	256	48	20	304	53	60	352	52	71
17	21	68	65	7	50	113	24	53	161	56	52	209	64	48	257	48	47	305	53	52	353	52	55
18	21	34	66	7	53	114	24	25	162	56	72	210	64	39	258	48	49	306	53	72	354	52	42
19	21	60	67	7	25	115	24	68	163	56	71	211	64	59	259	39	59	307	53	71	355	52	20
20	21	52	68	7	68	116	24	34	164	56	55	212	64	50	260	39	50	308	53	55	356	52	47
21	21	72	69	7	34	117	24	60	165	56	42	213	64	53	261	39	53	309	53	42	357	52	49
22	21	71	70	7	60	118	24	52	166	56	20	214	64	25	262	39	25	310	53	20	358	72	71
23	21	55	71	7	52	119	24	72	167	56	47	215	64	68	263	39	68	311	53	47	359	72	55
24	21	42	72	7	72	120	24	71	168	56	49	216	64	34	264	39	34	312	53	49	360	72	42
25	21	20	73	7	71	121	24	55	169	29	46	217	64	60	265	39	60	313	25	68	361	72	20
26	21	47	74	7	55	122	24	42	170	29	64	218	64	52	266	39	52	314	25	34	362	72	47
27	21	49	75	7	42	123	24	20	171	29	67	219	64	72	267	39	72	315	25	60	363	72	49
28	17	7	76	7	20	124	24	47	172	29	48	220	64	71	268	39	71	316	25	52	364	71	55
29	17	23	77	7	47	125	24	49	173	29	39	221	64	55	269	39	55	317	25	72	365	71	42
30	17	24	78	7	49	126	38	56	174	29	59	222	64	42	270	39	42	318	25	71	366	71	20
31	17	38	79	23	24	127	38	29	175	29	50	223	64	20	271	39	20	319	25	55	367	71	47
32	17	56	80	23	38	128	38	46	176	29	53	224	64	47	272	39	47	320	25	42	368	71	49
33	17	29	81	23	56	129	38	64	177	29	25	225	64	49	273	39	49	321	25	20	369	55	42
34	17	46	82	23	29	130	38	67	178	29	68	226	67	48	274	59	50	322	25	47	370	55	20
35	17	64	83	23	46	131	38	48	179	29	34	227	67	39	275	59	53	323	25	49	371	55	47
36	17	67	84	23	64	132	38	39	180	29	60	228	67	59	276	59	25	324	68	34	372	55	49
37	17	48	85	23	67	133	38	59	181	29	52	229	67	50	277	59	68	325	68	60	373	42	20
38	17	39	86	23	48	134	38	50	182	29	72	230	67	53	278	59	34	326	68	52	374	42	47
39	17	59	87	23	39	135	38	53	183	29	71	231	67	25	279	59	60	327	68	72	375	42	49
40	17	50	88	23	59	136	38	25	184	29	55	232	67	68	280	59	52	328	68	71	376	20	47
41	17	53	89	23	50	137	38	68	185	29	42	233	67	34	281	59	72	329	68	55	377	20	49
42	17	25	90	23	53	138	38	34	186	29	20	234	67	60	282	59	71	330	68	42	378	47	49
43	17	68	91	23	25	139	38	60	187	29	47	235	67	52	283	59	55	331	68	20			
44	17	34	92	23	68	140	38	52	188	29	49	236	67	72	284	59	42	332	68	47			
45	17	60	93	23	34	141	38	72	189	46	64	237	67	71	285	59	20	333	68	49			
46	17	52	94	23	60	142	38	71	190	46	67	238	67	55	286	59	47	334	34	60			
47	17	72	95	23	52	143	38	55	191	46	48	239	67	42	287	59	49	335	34	52			
48	17	71	96	23	72	144	38	42	192	46	39	240	67	20	288	50	53	336	34	72			

Figure A3: The connections between the brain regions R1 and R2 corresponding to FNC features

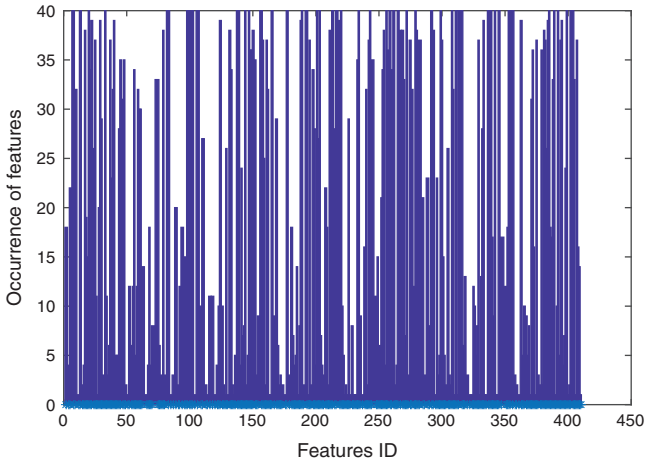

Figure A4: The occurrence of 410 features by the MLA method, where the features with index 1 to 378 are FNC features and the rest are SBM features